Diverse organic carbon dynamics captured by radiocarbon analysis of distinct compound classes in a grassland soil

Katherine E. Grant[1*], Marisa N. Repasch[1,2,3], Kari M. Finstad[1], Julia D. Kerr[1], Maxwell Marple[1], Christopher J. Larson[1,4], Taylor A. B. Broek[1,5], Jennifer Pett-Ridge[1,6], and Karis J. McFarlane[1]

[1]Physical and Life Sciences Directorate, Lawrence Livermore National Laboratory, Livermore, CA 94550, USA
[2]Institute of Arctic and Alpine Research, University of Colorado, Boulder, CO, USA
[3]Earth and Planetary Sciences, University of New Mexico, Albuquerque, NM, USA
[4]Department of Earth and Environmental Science, University of Pennsylvania, Philadelphia, PA, USA
[5]National Ocean Sciences Accelerator Mass Spectrometry (NOSAMS) Facility, Woods Hole Oceanographic Institution Woods Hole, MA, USA
[6]Life and Environmental Sciences Department, University of California-Merced, Merced, CA, USA

Correspondence to: Katherine E. Grant (grant39@llnl.gov)

Abstract. Soil organic carbon (SOC) is a large, dynamic reservoir composed of a complex mixture of plant and microbe derived compounds with a wide distribution of cycling timescales and mechanisms. The distinct residence times of individual C components within this reservoir depend on a combination of factors, including compound reactivity, mineral association, and climate conditions. To better constrain SOC dynamics, bulk radiocarbon measurements are commonly used to trace biosphere inputs into soils and estimate timescales of SOC cycling. However, understanding the mechanisms driving the persistence of organic compounds in bulk soil requires analyses of SOC pools that can be linked to plant sources and microbial transformation processes. Here, we adapt approaches, previously developed for marine sediments, to isolate organic compound classes from soils for radiocarbon (^{14}C) analysis. We apply these methods to a soil profile from an annual grassland in Hopland, California (USA) to assess changes in SOC persistence with depth to 1 m. We measured the radiocarbon values of water extractable organic carbon (WEOC), total lipid extracts (TLE), total hydrolysable amino acids (AA), and an acid-insoluble (AI) fraction from bulk and physically separated size fractions (<2 mm, 2 mm–63 μm, and <63 μm). Our results show that Δ^{14}C values of bulk soil, size fractions, and extracted compound classes became more depleted with depth, and individual SOC components have distinct age-depth distributions that suggest distinguishable cycling rates. We found that AA and TLE cycle faster than the bulk soils and the AI fraction. The AI was the most ^{14}C depleted fraction, indicating it is the most chemically inert in this soil. Our approach enables the isolation and measurement of SOC fractions that separate functionally distinct SOC pools that can cycle relatively quickly (e.g., plant and microbial residues) from more passive or inert SOC pools (associated with minerals or petrogenic) from bulk soils and soil physical fractions. With the effort to move beyond SOC bulk analysis, we find that compound class ^{14}C analysis can improve our understanding of SOC cycling and disentangle the physical and chemical factors driving OC cycling rates and persistence.

1 Introduction

34

35   Soil organic carbon (SOC) is a large and complex terrestrial reservoir of Earth's organic carbon (OC) (Jobbágy and

36   Jackson, 2000). It is a highly dynamic and open pool with inputs from decaying plant material, living roots, and soil microbes,

37   and with losses driven by microbial activity that includes the degradation and transformation of compounds (Angst et al.,

38   2021). The results of these processes is a heterogenous mixture of organic compounds with different radiocarbon (^{14}C) ages

39   and reactivities (Lehmann and Kleber, 2015; Shi et al., 2020; Trumbore and Harden, 1997; Gaudinski et al., 2000; Mcfarlane

40   et al., 2013). This complexity obscures the mechanisms that control overall OC persistence in soils, resulting in a continued

41   debate over the degree to which environmental factors, physical protection, and chemical composition influence SOC reactivity

42   and persistence (Lützow et al., 2006; Lehmann et al., 2020; Schmidt et al., 2011).

43   Bulk analysis methods have not fully demonstrated how physical protection and chemical composition interact to

44   influence SOC persistence, and so novel organic matter characterization methods are necessary to shed light on how different

45   compound classes of OC are preserved in soils and through what mechanisms. For example, we need to understand how the

46   chemical structure of OC influences interactions with mineral surfaces, such as aggregation or sorption, as well as how the

47   environment influences the decomposition and resource availability of certain OC compounds and functional groups.

48   However, it has been difficult to isolate, identify, and quantify pools of OC that directly link to in-situ OC chemical compounds

49   (Von Lutzow et al., 2007). Therefore, multiple approaches are needed to fully understand the interplay between chemical

50   compound persistence and mineral interaction functions in soil.

51   One approach used to investigate the controls on SOC persistence is to separate soil into operationally defined carbon

52   pools (e.g., size or density fractions) and characterize the resulting fractions. This approach has demonstrated that association

53   of OC with soil minerals is a critical mechanism for C stabilization (Vogel et al., 2014; Mikutta et al., 2007), as ^{14}C data

54   indicate that some mineral-associated C can persist for thousands of years (Torn et al., 2009). However, ^{13}C labelling

55   experiments show that some mineral-associated C cycles quickly, within months to years (Keiluweit et al., 2015; De Troyer

56   et al., 2011). Likely, some biomolecules form strong associations with mineral surfaces, such as long-chain lipids with iron

57   oxides (Grant et al., 2022), while other compounds only loosely associate with minerals (e.g., through hydrophobic interactions

58   with other OC compounds) (Kleber et al., 2007). Therefore, mineral-associated OC isolated using soil physical fractionation

59   methods remains a heterogenous mixture of OC molecules that have a distribution of turnover times, rather than a homogenous

60   and intrinsically stable SOC pool (Stoner et al., 2023; Van Der Voort et al., 2017).

61   Another approach that can yield finer resolution of OC turnover than traditional techniques is to isolate and measure the

62   isotopic signature of specific compounds (Von Lutzow et al., 2007). In marine and riverine systems, compound specific

63   radiocarbon analysis (CSRA) has been used monitor the degradation of organic carbon through the marine water column (Loh

64   et al., 2004), characterize marine particulate OC (Hwang and Druffel, 2003), constrain terrestrial OC burial and export from

65   river systems (Galy et al., 2015; Galy et al., 2008; Repasch et al., 202nd determine effect of OC export and burial on

66   precipitation patterns and climate (Hein et al., 2020; Eglinton et al., 2021). Different types of compounds including plant or

67   microbial lipid biomarkers (Douglas et al., 2018; Huang et al., 1996), amino acids (Bour et al., 2016; Blattmann et al., 2020),

68   lignin (Feng et al., 2017; Feng et al., 2013), certain carbohydrate compounds (Kuzyakov et al., 2014; Gleixner, 2013), and

69   pyrogenic carbon (Coppola et al., 2018) can be isolated and analysed for ^{14}C leading to a more detailed understanding of the

70   cycling of targeted compounds in the environment. Each of these specific compounds can provide information related to the

71   persistence and/or source of the OC in soils. For instance, lipids are found in plant cell walls and microbial cell membranes

72   and used for energy storage. Amino acids are necessary for protein formation and enriched in nitrogen (N) relative to other

73   plant and microbial residues. These two compound classes not only have diverse chemical reactivities which allows for insight

74   into chemical compound persistence. Understanding the abundance and age of these two biomarkers in soils can help

75   differentiate the source of C used by soil microbes for metabolism and growth (e.g., new C inputs vs older, recycled soil C) as

76   well as the transformation pathways that yield persistent SOC.

77   Recently, CSRA approaches developed for these environments have been applied to soil showing promise for identifying

78   distinct ages of plant and microbial biomarkers in SOC (Gies et al., 2021; Grant et al., 2022; Van Der Voort et al., 2017; Jia

79   et al., 2023; Douglas et al., 2018). Most of these CSRA studies applied to SOC have targeted specific, individual biomarkers

80   in soils, which generally contribute less than 5% of the entire carbon pool (Lützow et al., 2006; Kögel-Knabner, 2002). This

81   approach can be can be too specific to elucidate wholistic mechanisms for SOC persistence and turnover that pertain to the

82   majority of SOC. While individual biomarker ages, such as single ages of a particular lipid or single amino acid, can be useful

83   in some contexts, comprehensive understanding carbon compound class persistence is vital for understanding and modelling

84   the soil carbon reservoir's vulnerability to degradation.

85   To strike a balance between too specific and too broad, some researchers have characterized broader compound classes

86   rather than isolating a single biomarker. For example, this ^{14}C-compound class approach has been applied to marine dissolved

87   and particulate OC with a range of compounds, such as total lipids and total amino acids, to provide a broader understanding

88   of OC persistence in oceans (Wang et al., 2006; Wang et al., 1998; Loh et al., 2004). Wang et al. (1998) established a sequential

89   extraction procedure to analyse ^{14}C abundance of total lipids, amino acids, carbohydrates, and a residual acid insoluble fraction

90   from marine POC and sediments. This approach yielded distinct differences in ^{14}C age and abundance of the amino acids,

91   lipids, and the acid insoluble fraction in POC from the marine water column and sediment, as well as in costal verses open

92   ocean environments. Loh et al. (2004) found the lipid fraction of dissolved OC and POC to be the oldest fraction measured in

93   both the Atlantic and Pacific oceans, while the acid insoluble fraction was intermediate in age, and the amino acids and

94   carbohydrates contained a significant contribution of modern carbon. Wang and Druffel (2001) also used this approach and

95   found that the lipids were the oldest compound class from sediments in the Southern Ocean, but the acid insoluble residue was

96   very similar in age to the lipid fraction. These studies suggest that compound classes can have independent cycling rates, but

97   these cycling rates can be influenced by OC environment.

98   Here, we apply a ^{14}C compound class approach to soils to more broadly understand SOC turnover mechanisms. We

99   characterize the distribution and ^{14}C age of multiple SOC pools with depth in a well-studied Californian grassland, using soil

100   physical fractionation (Mcfarlane et al., 2013; Poeplau et al., 2018) and modified compound class extraction methods

101 previously detailed for marine sediments (Wang et al., 1998). We measured the radiocarbon values of water extractable organic

102 carbon (WEOC), total lipid extracts (TLE), total hydrolysable amino acids (AA), and an acid-insoluble (AI) fraction from bulk

103 and physically separated size fractions (bulk soil, sand, and silt+clay). We expected the TLE to be older than its source fraction

104 (bulk soil, sand, or silt+clay), to be older with depth as the decline in plant inputs necessitates recycling and use of older SOC,

105 and to be older in the silt+clay fraction as its high surface area should result mineral-OC associations that protect SOC from

106 soil microbes. We expected the AA to cycle faster than the TLE fraction and the bulk SOC pool based on the young ^{14}C ages

107 found for AA extracted from in marine sediments (Wang et al., 1998; Wang and Druffel, 2001), but hypothesized that recycling

108 of amino acids at depth by soil microbes might result in an increase in the age of AA below 50 cm. Finally, we expected AI to

109 have old C, similar to the TLE, as seen found in marine sediments (Wang et al., 1998). Here, we describe the relative abundance

110 and radiocarbon content of total lipid and amino acid compound class extracts and compare carbon storage and cycling rates

111 within physical soil size fractions. These data provide a foundation for the continued application of compound class ^{14}C work

112 to the understanding and modelling of soil OC persistence.

2 Materials and Methods

2.1 Site and Sample Description

115 Soil samples were collected from the University of California's Hopland Research and Extension Center (HREC) in January

116 2022. The site is an annual grassland with a Mediterranean-type climate; mean annual precipitation (MAP) averages 940 mm

117 per year and the mean annual temperature is 15˚C (Nuccio et al., 2016). The underlying geology consists of mixed sedimentary

118 rock of the Franciscan formation. The soils are designated Typic Haploxeralfs of the Witherall-Squawrock complex (Soil

119 Survey Staff, 2020). The samples were collected from the "Buck" site (39.001º, -123.069º) where the vegetation is dominated

120 by annual wild oat grass, *Avena barbata* (Kotanen, 2004; Bartolome et al., 2007). Soils were collected from a freshly dug soil

121 pit at four depths: 0–10 cm, 10–20 cm, 20–50 cm, and 50–100 cm. Samples were stored in sealed plastic bags at ambient

122 temperature and transported to the laboratory in Livermore, CA. Soil samples were air dried, homogenized, and sieved to 2

123 mm, with the >2 mm fraction retained for further analysis. Samples were subdivided for soil characterization, physical size

124 separations, chemical compound extractions, and density fractionation.

2.2 Physical Fractionation

126 To compare compound classes between mineral-associated OC and mineral-free OC, we used a salt-free and chemical-free

127 method for isolating the mineral-associated organic matter from the free particulate organic matter (Fig. 1a). Under the

128 assumption that mineral-associated carbon is primarily found in the silt+clay (<63 μm) particle size fraction, we used a size

129 fractionation sieving method where air-dried samples were dry-sieved into three size fractions: bulk soil (<2 mm), sand (2 mm

130 - 63 μm), and silt+clay (<63 μm) (Lavallee et al., 2020; Poeplau et al., 2018). Additionally, because the majority of free

131 particulate organic carbon (POC) is contained in the sand faction, we used a "water density" separation to remove the low

132 density POC from the mineral matter in this fraction, resulting in a POC ($<1g$ mL^{-1}) fraction and a POC-free ($>1g$ mL^{-1}) sand

133 faction.

134 To further characterize these soils and aid in interpretation of our data, we compared the size fractionated samples to samples

135 separated by density using sodium polytungstate (SPT-0 adjusted to a density of 1.65 g ml^{-1}) (Poeplau et al., 2018) (see SI

136 Section 1.1 for detailed methods). We chose to focus our compound class extraction efforts on size fractionated samples to

137 avoid chemical alteration of SOC during exposure to SPT.

138 To constrain any contributions of parent materials to SOC, we processed and analyzed the rock fraction (> 2mm) (Agnelli et

139 al., 2002; Trumbore and Zheng, 1996). Rocks were washed with 18.2 MΩ water in an ultrasonic bath to remove surface

140 contamination, rinsed with 1N HCl to remove any additional weathered material loosely adhered to the surface, dried at 60°C,

141 then manually crushed.

142 A large, representative aliquot (~10 g) of the bulk and each physical fraction were ball milled and measured for total organic

143 carbon (TOC, wt %), C/N ratio, δ^{13}C and Δ^{14}C (Section 2.6). In addition, we analyzed the bulk soils at each depth with nuclear

144 magnetic resonance (^{13}C NMR) to assess the broad structural complexity of the OC in the bulk soil (SI Section 2).

145
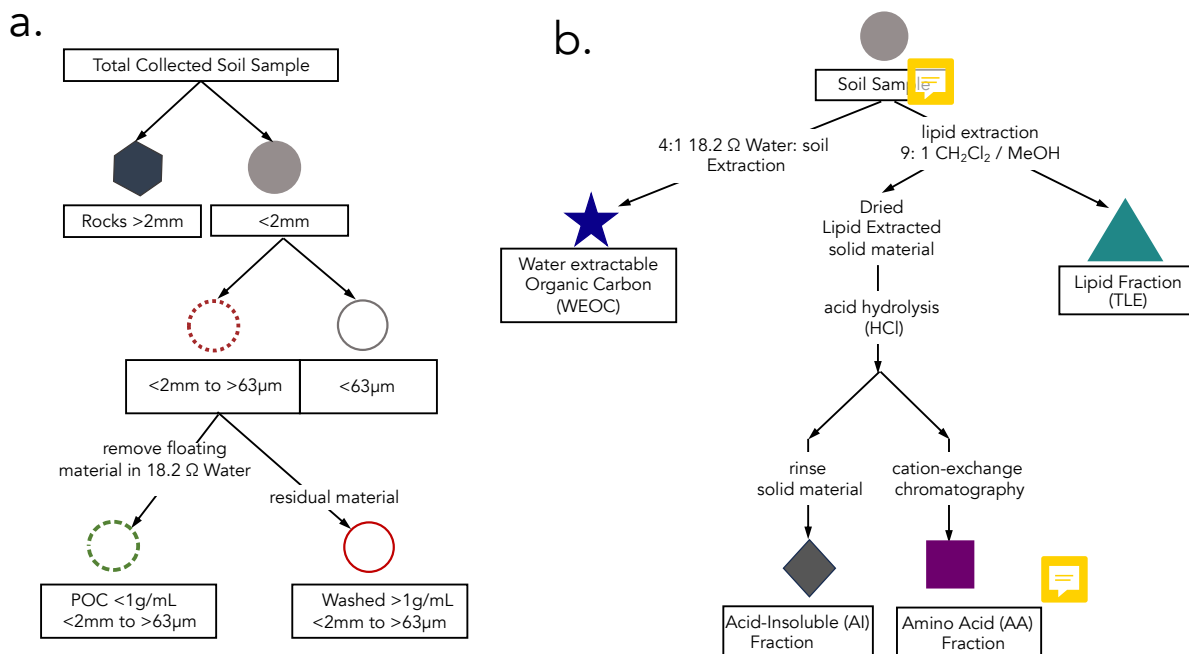
146

147 **Figure 1: Schematics of protocols used in this study for a) fractionation by size and b) extraction of targeted compound classes.**

148

149 **2.3 Water-extractable organic carbon (WEOC)**

150 The water-extractable organic carbon (WEOC) fraction was collected from 80 g of bulk soil with 18.2 MΩ water using a 4:1

151 water to soil ratio (Van Der Voort et al., 2019; Lechleitner et al., 2016; Hagedorn et al., 2004). Saturated soil samples were

152 shaken for 1 hour and then filtered through a pre-rinsed 0.45 μm polyethersulfone (PES) Supor filter under vacuum. An aliquot

153 was taken for dissolved organic carbon (DOC) measurement on a Shimadzu TOC-L combustion catalytic oxidation instrument.

154 Sample concentrations were determined using a nine-point DOC calibration curve ranging from 0-200 mgC L^{-1}. The WEOC

155 fraction was dried using a Labconco CentriVap centrifugal drying system at 40°C and subsequently transferred with 0.1N HCl

156 into pre-combusted quartz tubes to eliminate any inorganic carbon dissolved in the aqueous fraction. The acidified WEOC

157 fractions were then dried down using the CentriVap. Dried samples were flame sealed under vacuum (Section 2.6) for

158 subsequent carbon isotope analyses.

2.4 Total Lipid Extraction (TLE)

161 Total lipids (TLE) were extracted from the soil samples using an Accelerated Solvent Extraction (ASE) system (Dionex 350,

162 Thermo Scientific) in duplicate. The TLE was extracted from the bulk, sand, silt+clay, and the dense fraction (> 1.65 g ml^{-1};

163 DF). An aliquot of 10–30 g of soil was loaded into an a stainless-steel ASE extraction cell depending on TOC content

164 (Rethemeyer et al., 2004). The ASE was set to extract the sample for 5 minutes with a holding temperature of 100°C at 1500

165 PSI. Lipids were extracted using a 9:1 ratio of dichloromethane (DCM or syn: methylene chloride) to methanol (Wang et al.,

166 1998; Van Der Voort et al., 2017; Grant et al., 2022). The TLE was dried under constant ultra-pure N$_2$ flow at 40°C using a

167 nitrogen dryer (Organomation Multivap Nitrogen Evaporator). The TLE was resuspended in ~5ml of 9:1 DCM:Methanol then

168 transferred to pre-combusted quartz tubes, dried again, and analyzed for ^{14}C as described below (Section 2.5). Total CO$_2$

169 produced by the combustion of the TLE was measured manometrically on the ^{14}C vacuum lines during graphitization. Process

170 blank samples were analyzed with each batch (SI Section 3.1).

2.5 Amino Acid (AA) Extraction

173 Amino acids (AA) were extracted from the lipid-extracted residual bulk and silt+clay size fraction with an acid hydrolysis

174 procedure, desalted, and isolated with cation exchange chromatography using methods modified from those used in marine

175 systems (Wang et al., 1998; Ishikawa et al., 2018; Blattmann et al., 2020). Briefly, a 500 mg soil aliquot was hydrolyzed with

176 6N HCl (ACS grade) under an N$_2$ atmosphere for 19-24 hours at 110°C. After hydrolysis, amino acids in solution were

177 separated from the solid acid insoluble (AI) fraction via centrifugation for 5 minutes at 2500 rpm. The AI fraction was

178 subsequently washed at a minimum three additional times with 0.2N HCl to ensure complete AA recovery. The supernatant

179 was collected in a single pre-combusted vial and then filtered through a pre-combusted quartz wool fiber plug to remove

180 extraneous sediment particles. The filtered hydrolysate was dried using a CentriVap at 60°C for 4 hours. The dried supernatant

181 was redissolved in 1 ml 0.1N HCl and loaded onto a preconditioned resin column (BioRad 50WX8 200-400 mesh resin) to

182 isolate the AA from other hydrolyzed organic matter and remove excess chloride. Details of the procedure can be found in

183 Ishikawa et al., 2018. Briefly, once the sample was loaded on the column, it was rinsed with three bed volumes (~6 ml) of 18.2

184 MΩ H_2O. The free AA were eluted with 10 ml of 2N ammonium hydroxide (NH_4OH), then transferred into pre-baked quartz

185 tubes, dried at 60°C in the CentriVap, and finally sealed and combusted for isotopic analysis. The remaining rinsed solid

186 residual after hydrolysis is the acid-insoluble (AI) fraction. These are processes as a solid sample for isotopic analysis.

187

2.6 Isotopic and elemental analysis

189 All samples were analyzed for radiocarbon (^{14}C) at the Center for Accelerator Mass Spectrometry (CAMS) at Lawrence

190 Livermore National Lab (LLNL) in Livermore, California. Samples were either measured on a 10 MV Van de Graaf FN or

191 1MV NEC Compact accelerator mass spectrometer (AMS) (Broek et al., 2021), with average errors of $F^{14}C = 0.0035$. For

192 solid soil analysis, 10 to 250 mg of ground material was weighed into a pre-combusted quartz tubes along with 200 mg CuO

193 and Ag, flame sealed under vacuum, then combusted at 900°C for 5 hours. The CO_2 was reduced to graphite on preconditioned

194 iron powder under H_2 at 570°C (Vogel et al., 1984). Measured ^{14}C values were corrected using $\delta^{13}C$ values and are reported

195 as age-corrected $\Delta^{14}C$ values using the following the conventions of Stuiver and Polach (1977). Extraneous C was quantified

196 for the TLE and AA extractions (SI Table 4 and SI Section 3). For ease of reference, we included conventional radiocarbon

197 ages in our figures and tables. We quantified turnover times using the single pool turnover model described in Sierra et al.

198 (2014) and Van Der Voort et al. (2019) and explained in detail in Trumbore (2000) and Torn et al. (2009). This approach

199 generates two solutions for pools with $\Delta^{14}C > 0$ ‰, one corresponding to each side of the atmospheric ^{14}C-CO_2 curve over the

200 last 70 years (Hua et al., 2022). Unfortunately, we cannot identify the correct solution (Mcfarlane et al., 2013; Trumbore,

201 2000), especially for TLE and AA fractions from the top 20 cm, as we do not have multiple time points or additional constraints

202 such as pool-specific input or decomposition rates. Therefore, our data analysis and interpretations rely on the reported $\Delta^{14}C$

203 values. All individual ^{14}C measurements used in this study are listed in the Supplementary Information (SI Table 1 and 2).

204 For each solid sample, a dried homogenized aliquot was analyzed for TOC concentration and $\delta^{13}C$ using an elemental analyzer

205 (CHNOS) coupled to an IsoPrime 100 isotope ratio mass spectrometer at the Center for Stable Isotope Biogeochemistry (CSIB)

206 at the University of California, Berkeley. Samples are assumed to have no inorganic carbon based on acid leaching tests and

207 previously published ^{14}C work at this site (Finstad et al, 2023, Foley et al., 2023). $\delta^{13}C$ was measured in duplicate for each

208 solid sample and errors represent the standard deviation of the mean. $\delta^{13}C$ values of WEOC, TLE, and AA extracts were

209 measured on a split of the cryogenically purified CO_2 and were analyzed at the Stable Isotope Geosciences Facility at Texas

210 A&M University on a Thermo Scientific MAT 253 Dual Inlet Stable Isotope Ratio Mass Spectrometer (SI Table 1).

211

2.7 Data analysis

213 Data was analyzed using MATLAB version R20223 and R v. 3.614 (R Core Team, 2019). Linear regressions were calculated

214 between the sample depth mid-point and $\Delta^{14}C$ values from both the size fractions as well as the extracted compounds (WEOC,

215 TLE, AA, AI) from the different size fractions. This was done to directly compare the difference in $\Delta^{14}C$ value between the

216 compound classes. Correlation coefficients, p-values and r^2 are provided in SI Table 3. Analysis of Variance (ANOVA) was

217 used to assess differences in $\Delta^{14}C$ with depth, between TLE and AA, and between soil fractions. ANOVA tests were performed

218   in R v. 3.614 (R Core Team, 2019). In the text, results are reported as means followed by one standard error when n = 2 or 3

219   or by analytical error when n = 1.

220

221   **3 Results**

222   **3.1 Radiocarbon values and characterization of the physical fractions**

223   We used soil size and density fractionation to separate the bulk soil into fractions with different degrees of mineral protection.

224   Radiocarbon content for the bulk soil, sand, and silt+clay (SI Table S3) became more ^{14}C depleted (older) with increasing

225   depth (Table 1, Fig. 2). SOC in the silt+clay was consistently younger than in the bulk soil, with the average difference in Δ^{14}C

226   values increasing from 4‰ at the surface to 87‰ at depth.

227

228 **Table 1. Carbon concentrations, mass fractions, and radiocarbon values for the size separations from the Buck Pit**

229

Depth	bulk (<2mm)		sand-sized (2mm to 63μm)			POC-free >1g mL⁻¹		POC <1 gmL⁻¹		silt+clay (<63μm)		
	%OC	Δ¹⁴C ± err (‰)	mass f	%OC	Δ¹⁴C ± err (‰)	%OC	Δ¹⁴C ± err (‰)	%OC	Δ¹⁴C ± err (‰)	mass f	%OC	Δ¹⁴C ± err (‰)
0-10 cm	3.14	31 ± 3	0.71	2.68	25 ± 3	2.08	25 ± 3	25.69	19 ± 3	0.29	4.25	34 ± 3
10-20 cm	1.22	-22 ± 3	0.69	0.94	-38 ± 3	0.77	-35 ± 3	25.99	-5 ± 3	0.31	1.84	-13 ± 3
20-50 cm	0.50	-116 ± 3	0.75	0.39	-142 ± 3	0.38	-149 ± 2	n.m.	4 ± 3	0.25	0.85	-79 ± 3
50-100 cm	0.25	-468 ± 3	0.79	0.23	-496 ± 3	0.18	-510 ± 2	n.m.	-10 ± 3	0.21	0.35	-380 ± 3

230

231
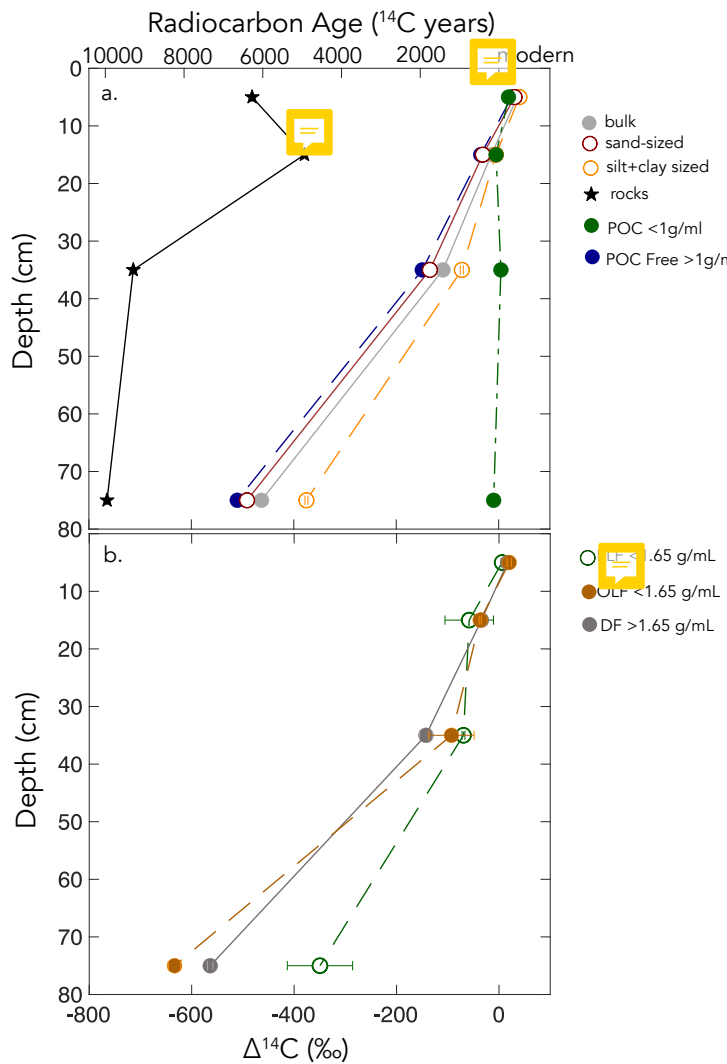
Figure 2: Δ^{14}C values by depth for a) size-fractions and b) density-fractions from the Buck soil pit. Conventional ^{14}C ages are provided for reference.

In the sand fraction, the Δ^{14}C values of POC were consistently near current atmospheric values (2 ± 3‰) and were not significantly correlated with depth. In contrast, the Δ^{14}C values of the POC-free sand-sized fraction declined with depth (+25 ± 3‰ to -510 ± 2‰, p = 0.006) and were indistinguishable from the POC-free sand fraction (Fig. 2). Density fractionation of the bulk soil resulted in most of the sample mass (> 98%) and OC (75–83%) recovered in the DF at all depths (SI Fig. S2).

240

3.2 Compound Class results from bulk soil and silt+clay

In both the bulk soil and silt+clay fraction, the extracted compound classes became ^{14}C-depleted with depth except for the WEOC, which had ^{14}C values that reflected C inputs recently fixed from the atmosphere throughout the soil profile (Fig. 2; SI tables). The $\Delta^{14}C$ values of the WEOC ranged from $+14 \pm 4$‰ at the surface to -46 ± 4‰ at depth, and the DOC concentrations ranged from 43.2 to 6.7 mg C g soil^{-1} at the surface and at depth, respectively.

The TLE from the bulk soil had $\Delta^{14}C$ values that range from 17 ± 27 to -208 ± 6‰ (n = 2; $\pm$ SE) in the surface and deepest sample, respectively. In comparison, the TLE from the silt+clay fraction was modern at the surface and became more ^{14}C depleted with depth (p < 0.001), from $+46 \pm 4$ to -204 ± 36 ‰. The slopes of the linear regressions of $\Delta^{14}C$ with depth were indistinguishable in TLE from the bulk soil and silt+clay. In addition, the TLE from the bulk TLE and silt+clay fraction TLE (SI Tables) had very similar $\Delta^{14}C$ values, but the bulk soil had less lipid-C extracted during each experiment (280 μg g C^{-1} in the 0-10 cm vs. 150 μg g C^{-1}; SI Table 2).

The $\Delta^{14}C$ values of the AA extracted from the bulk soil ranged from 54 ± 5 to -183 ± 24 (n = 2, SE) with depth (Fig. 3, SI Table S3). Similarly, the $\Delta^{14}C$ value of the AA fraction extracted from silt+clay declined with depth from $+60 \pm 3$‰ (n = 2, SE) at the surface to -106 ± 4 ‰ (n = 2, SE) at 50-100 cm depth. The slopes of the AA extracted from the bulk and silt+clay-size fractions were statistically different, indicating that the AA extracted from the bulk soil became more depleted with depth than that extracted from the silt+clay (SI Table S3). Furthermore, AA fractions were enriched in ^{14}C values relative to the TLE or AI fraction (p < 0.01 for bulk soil and p < 0.05 for silt+clay).

The AI fraction was the oldest fraction found in our study at each depth. The $\Delta^{14}C$ values of the AI fraction ranged from -5 ± 2‰ to -633 ± 2‰ (analytical error, n=1) and declined with depth (p < 0.01 for bulk soil and silt+clay; Fig. 3; SI Table S3).
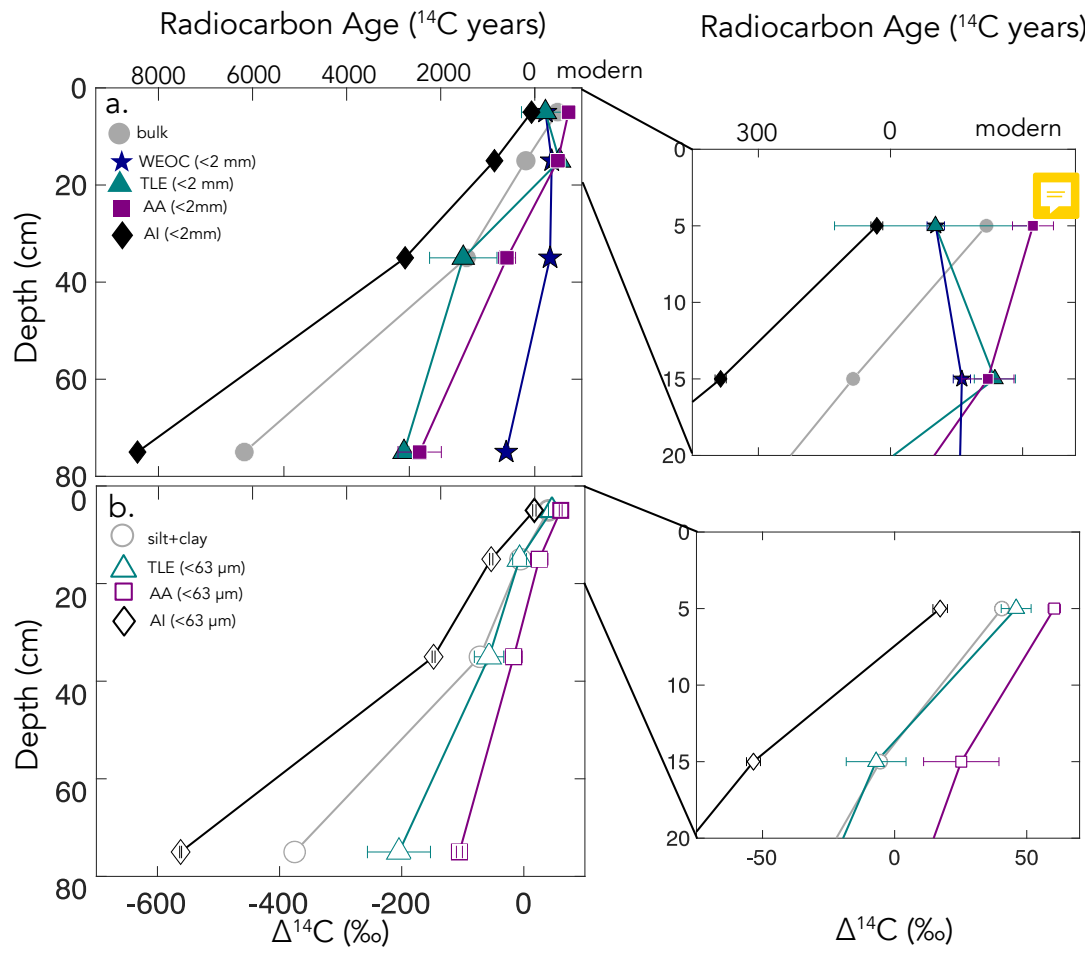
Figure 3: $\Delta^{14}C$ by depth for a) bulk soil and four compound class fractions extracted from bulk soil for the entire depth profile with the inset of the top 20 cm and b) the silt+clay (<63 μm) fraction and three compound classes extracted from the silt+clay for the entire depth profile with the inset of the top 20 cm. For TLE and AA fractions (n=2) and error bars represent the standard error from duplicate measurements. For the <2mm, WEOC, and AI fractions (n=1) and error bars represent analytical error. Error bars are smaller than the marker width where not shown.

4 Discussion

4.1 Variability of compound classes in bulk soils and fractions

We measured radiocarbon content of four distinct soil chemical extracts: water extractable organic carbon (WEOC), total lipid extract (TLE), free amino acids (AA), and the acid insoluble fraction (AI), which had distinct $\Delta^{14}C$ values compared to the initial soil fraction each was extracted from (bulk or silt+clay; Fig. 4a and 4b). As expected, $\Delta^{14}C$ values of TLE, AA, and AI became more depleted with depth (Fig. 2). More interestingly, the differences between the ^{14}C content of bulk soil and the extracted compounds were not consistent with depth (Fig. 4). This divergence in $\Delta^{14}C$ values reflects differences in turnover

276 times among compound classes, which can be influenced by the sources of OC to each of these pools and by differences in the

277 stabilization mechanisms protecting those compounds from decay. In this annual grassland, plant inputs should have a greater

278 influence on SOC pools near the surface, which we confirmed with near modern Δ^{14}C signatures in the 0-10 cm depth for all

279 compound classes and size-fractions (Fig. 3b and 3c). However, at deeper depths, new vegetation inputs should be less readily

280 available, which results in more depleted Δ^{14}C signatures at depth and could necessitate microbial use and recycling of older

281 SOC.

282 We found that, averaged across depths, the Δ^{14}C values of the TLE were more depleted than those of the AA, though both

283 compound classes were more enriched in Δ^{14}C than the bulk soil or silt+clay that they were extracted from. AAs are the

284 precursors of proteins and found in both plant and microbial biomass. The extracted AAs are hydrolysed proteins can be from

285 both plant material or microbial biomass within the soil sample (Blattmann et al., 2020), so our measurements likely reflect a

286 combination of both plant- and microbially-derived AAs. As in marine studies, we found the AAs to be the youngest compound

287 class fraction (of the TLE and AI) in these soils. The AA pool likely reflects a more actively cycling microbial pool especially

288 at depth, as AA are enriched in nitrogen compounds and likely microbes are both mining and recycling these compounds

289 (Moe, 2013). The divergence from bulk ^{14}C values indicate that even at depth in the soil, the AAs are either continuously

290 replenished from transport of AAs from surface horizons or re-synthesized with relatively ^{14}C enriched sources such as the

291 WEOC.

292 Based on published data for both soils and marine sediments, we expected the TLE to be older than both the AAs and the

293 bulk soil, however we found that all TLE samples, no matter what fraction we measured, were more ^{14}C enriched than the bulk

294 soil. TLE is composed of a continuum of lipids from plant and microbial materials, ranging from leaf waxes to microbial cell

295 structural components (Angst et al., 2021; Angst et al., 2016), that cycle at different rates and likely interact with mineral

296 surfaces. Previous studies where individual lipid biomarker Δ^{14}C values were measured in soils on either short chain or long

297 chain fatty acids found that there is a divergence in Δ^{14}C values between these two pools, with short chain lipids generally

298 having enriched ^{14}C values and long chain lipids having more depleted ^{14}C values (Grant et al., 2022; Van Der Voort et al.,

299 2017). For example, long-chain lipid biomarkers, primarily thought to be plant derived, had consistently older ^{14}C ages than

300 bulk soil (Van Der Voort et al., 2017). Short-chain lipids, which can be microbial or root derived (Rethemeyer et al., 2004),

301 were found to be younger than long-chain lipids throughout the soil profiles and younger than bulk soil at depth (Van Der

302 Voort et al., 2017). However, microbial cell wall lipid biomarkers (glycerol dialkyl glycerol tetraethers, GDGTs) had older

303 ^{14}C ages than bulk soils (Gies et al., 2021). With this consideration, our result of more enriched ^{14}C of the TLE could be an

304 indication of a predominance of short chain lipids and suggested higher abundance of microbially-derived lipids than plant-

305 derived lipids. However further study of specific lipid abundance (e.g., *n*-alkanes, fatty acids) in these soils are necessary, as

306 it is unclear to what degree lipids are older than bulk soils with depth because of preservation of these compounds through

307 mineral association or because of microbial use of aged OC sources for growth.

308
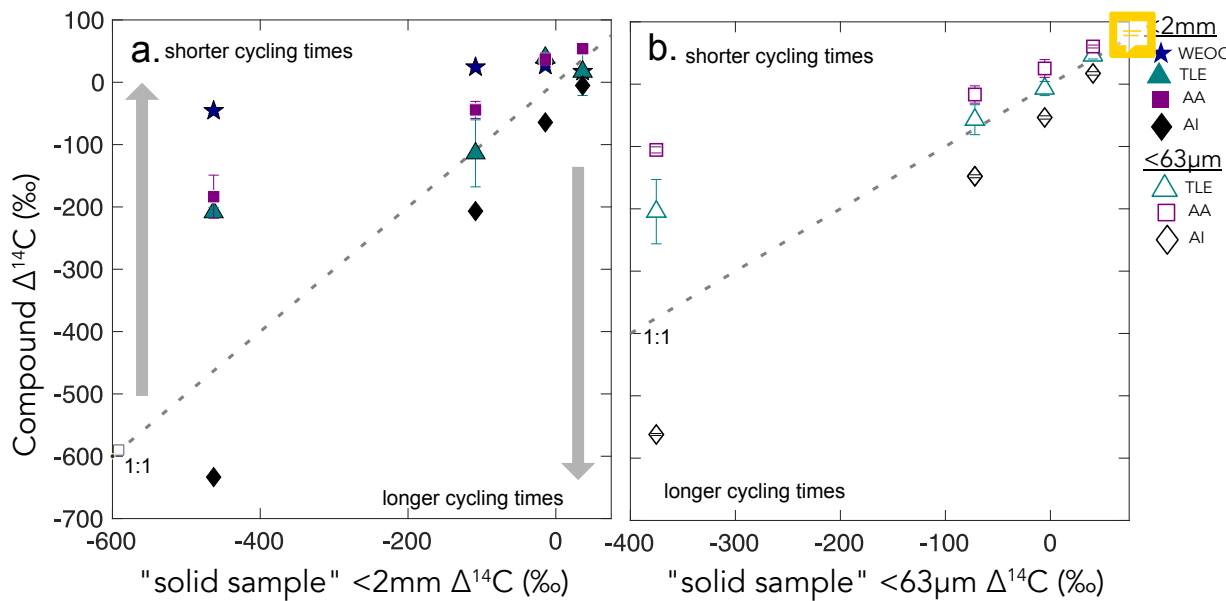
Figure 4. $\Delta^{14}C$ values of the three extracted compound classes (y-axis) compared to the $\Delta^{14}C$ values of the source fraction (x-axis) for a) bulk soil and b) silt+clay. The grey dashed lines show the 1:1 line where bulk sample $\Delta^{14}C$ equals compound class $\Delta^{14}C$. Gray arrows point to regions where data plot above or below the 1:1 line, suggesting that a given compound class has shorter and longer carbon turnover times than bulk soil, respectively.

4.2 Fast cycling OC throughout the depth profile

WEOC (extracted from bulk soils) and POC ($<1g\ mL^{-1}$ floated off the sand-size fraction) had the most enriched $\Delta^{14}C$ values throughout the soil profile, reflecting a predominance of modern carbon from plant detritus and root exudates to these pools. WEOC fractions can comprise a complex mixture of molecules with different structures (Hagedorn et al., 2004; Bahureksa et al., 2021), which are common only in their ability to be mobilized and dissolved in water. WEOC can mobilize and percolate down the soil profile with sufficient precipitation to allow vertical transport. Both the POC and WEOC fractions supply OC that is readily accessible for microbial degradation and microbial utilization – resulting in the rapid turnover and relatively high $\Delta^{14}C$ values of these two pools (Marin-Spiotta et al., 2011). Occurrence of young OC in deep soils may be driven by microbial uptake of this young and bioavailable DOC or POC. Additionally, we found that the free light-density fractions were depleted in ^{14}C relative to the WEOC and POC (Fig. 5). We suspect this is due to colloidal particles in the FLF, which are not dispersed or dense enough to settle in the SPT.

The study site has a Mediterranean climate, and these soils undergo seasonal wetting and drying cycles. These cycles may intensify in the future (Swain et al., 2018), potentially shifting the composition or amount of OC that percolates down the soil column. When soil is already moist, subsequent rainfall may mobilize both OC and colloidal sized mineral material from reducing conditions which may interact to form stable mineral-OC colloids which can enhance the transport of OC down the

330 soil profile and out of the system (Buettner et al., 2014). With prolonged dry periods, water soluble OC may be more

331 susceptible to microbial decomposition or oxidation. This seasonal wetting and drying mechanism likely controls what types

332 of organic matter are transported down the soil profile. Deeper in the soil profile, there is likely greater reactive mineral surface

333 area and less microbial activity, which can enhance carbon stabilization in subsoils (Homyak et al., 2018; Dwivedi et al., 2017;

334 Pries et al., 2023). Further research is needed to understand the effects of seasonal wetting and drying on the behaviour of

335 water-soluble OC in the soil profile.
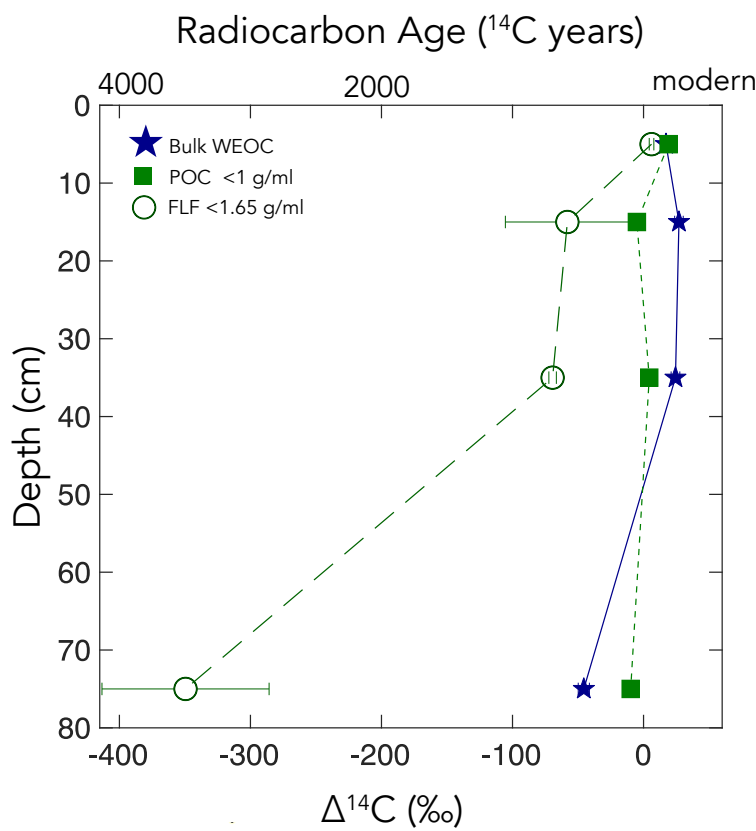
Figure 5: POC (floated from the sand, n = 1), FLF (from bulk soil, n = 3, and error bars indicate standard error on the mean), and WEOC (from bulk soil, n =1). $\Delta^{14}C$ values by depth. For POC and WEOC, error bars indicate analytical error are generally smaller than the symbols.

4.3 Compound class $\Delta^{14}C$ values in mineral-associated SOC

342 investigate the effect of mineral interaction on the $\Delta^{14}C$ values or persistence of the TLE, AA, and AI, we measured

343 these extracted compound classes from physical fractions intended to yield approximate mineral-associated carbon pools. We

344 focused primarily on the silt+clay size fraction as the physical fraction that best approximates a mineral-associated OC pool

345 derived from microbially processed plant inputs (Poeplau et al., 2018; Lavallee et al., 2020) and assume that after size

346   fractionation most of the free organic matter in the bulk soil was in the sand size fraction. We compared the silt+clay size

347   fraction Δ^{14}C values to the bulk Δ^{14}C values to determine if the material extracted from the isolated mineral-associated fractions

348   of the soil had greater OC persistence or if these compounds cycled indiscriminate of mineral association (Fig. 2).

349   While the TLE from the silt+clay and bulk soil had similar Δ^{14}C values, the AA from the silt+clay size fraction was

350   enriched in ^{14}C compared to the AA from bulk soil ($r^2 = 0.98$, $p<0.05$). This suggests that AAs cycle faster in the silt+clay

351   mineral pool than in the bulk soils. While mineral surfaces usually are thought to promote stability and persistence of OC, in

352   some soil systems, mineral associations may not be the single defining factor of OC persistence (Rocci et al., 2021) and could

353   have a more nuanced role influencing OC cycling in soils.

354   Our data suggests there is a continuum of compounds that exist with different ^{14}C values in the mineral-associated pool,

355   because in the silt+clay fraction, the TLE, AA, and AI have significantly different ^{14}C values (Fig. 4b).For instance, the

356   mineral-associated TLE and AA fractions are enriched in ^{14}C relative to the silt+clay fraction, suggesting both are cycling

357   faster than the average mineral associated pool. However, the AI from the silt+clay fraction is cycling slower than solid sample

358   it was extracted from, and when we compare the AI from the bulk soil to the AI from the silt+clay, the AI from the silt+clay

359   is slightly more ^{14}C enriched. This suggests that there is slight ^{14}C enrichment across all different compounds in the silt+clay

360   fraction.

361   We also compared the TLE extracted from the silt+clay to that extracted from the DF. The mineral-associated fraction is

362   not a uniformly defined pool and is also a consequence of the methodology used to separate the samples (Fig. 6). The DF TLE

363   Δ^{14}C is significantly older than the silt+clay TLE (Fig. 6b). While the DF TLE could be influenced by methodological

364   differences, such as artifacts from acidic SPT or grinding, it is still more ^{14}C enriched at depth than the TLE of the bulk soil

365   (Fig. 6), which is an indication that at the compound class level, lipids from mineral-associated OC pools still have multiple

366   cycling rates. This is complementary to findings from other studies where ^{14}C values from multiple different lipid biomarkers

367   are divergent from the bulk soils (Gies et al., 2021) and could indicate the necessity of looking at entire compound class pools.

368   These results warrant further investigation into the composition and age-distribution of compounds within mineral associated-

369   OC.
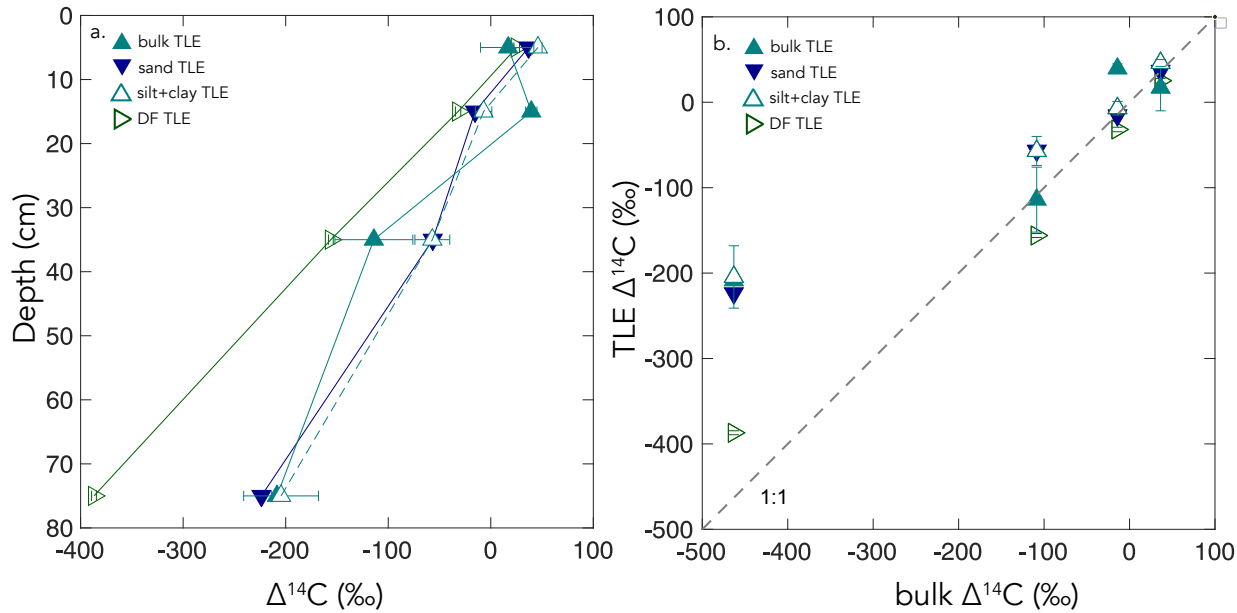
Figure 6: a) Δ^{14}C versus soil depth measured for TLE extractions from four soil size/density fractions. b) A comparison of the bulk soil Δ^{14}C values to the TLE from the four size/density fractions.

4.4 Persistent and Petrogenic OC

We found that the most ^{14}C depleted OC fraction measured at each soil depth was the AI (Fig. 3, 4), the residual sample after both the TLE and AA have been extracted (Wang et al., 1998; Wang et al., 2006). The AI fraction was far more depleted relative to the bulk samples (Fig. 2) than in other studies with marine acid-insoluble OC (Wang et al., 2006; Wang and Druffel, 2001). In the marine studies, the ^{14}C is found to be quite variable in age depending on sampling depth or location. The significant depletion of the AI in our soils suggests that these, chemically stable compounds, are not oxidized in soil. Importantly, our AI samples are older than other chemical and physical soil fractions in the soil, which is consistent with the finding that aromatic compounds can be difficult to degrade in in soils (Ukalska-Jaruga et al., 2019).

Since the AI cycles much more slowly than other components of this grassland soil, it is important to understand what structural components make up the AI and where these compounds are sourced from. The chemical structure of the AI fraction has been difficult to characterize. Hwang and Druffel (2003) argued that the AI is a lipid-like portion of the ocean OC. However, in soils, the AI can be composed of a mixture of lipid-like compounds and aromatic compounds (Silveira et al., 2008). In our soil, the ^{13}C-NMR spectra of the AI from 0-10 cm depth show a significant, broad peak in the 100–165 ppm range, indicative aromatics (SI Fig. 3) (Baldock and Preston, 1995; Baldock et al., 1997). While it is possible that some condensed aromatic compounds form during the hydrolysis procedure used to remove AAs, the AI may also contain naturally occurring aromatic compounds that could include pyrogenic or petrogenic OC.

17

390   The parent material of our site is a mixture of sandstone, shale, graywacke, and schist (Foley et al., 2022), so it is possible

391   that some of the OC in our soils is ancient, rock-derived, petrogenic carbon that has been incorporated into the soil profile

392   through pedogenesis progresses (Grant et al., 2023). Comparison of the AI to the rock (>2 mm) fraction shows that the AI is

393   younger than the OC contained in the rock fraction (SI Table 1), with the rock fraction $\Delta^{14}C$ values ranging from -481 to -

394   765‰. To calculate the contribution of OC_{petro} into the AI fraction, we used a binary mixing model with endmembers of

395   OC_{petro} and aged SOC based on the method in Grant et al. (2023). The OC_{petro} ^{14}C endmember was -1000 ‰ and we compared

396   and upper and lower range for the aged SOC ^{14}C values using the TLE and bulk ^{14}C values, respectively, from each depth. In

397   the AI extracted from the silt+clay fraction, the OC_{petro} contribution was 4–5% from 0–10 cm depth and 40–53 % in the 50–

398   100cm depth. In AI extracted from the bulk soil, the OC_{petro} contribution was 0–1 % in the 0–10 cm depth, and 17–44 % in the

399   50–100 cm depth. Therefore, while the AI fraction likely contains OC_{petro}, it is primarily composed of OC compounds derived

400   from more recent plant and microbial inputs that are highly resistant to acid hydrolysis either because of their chemical

401   structure or their strong associations with minerals.

402

403   **4.5 Comparison of Fractionated Samples**

404   We focus on the silt+clay fraction as an operationally defined mineral-associated OC pool. Numerous soil physical

405   fractionation schemes have been applied to soils and disparities in methods challenge interpretation and intercomparison of

406   results from different studies using different approaches. We compared our size-based approach to density fractionation of our

407   soils to aid in interpretation and comparability of our findings to other studies. Our silt+clay fraction had higher $\Delta^{14}C$ values

408   than the sand, POC-free sand, and the DF. Our silt+clay fraction may include free organic matter that passed through the 63

409   μm sieve but that would have floated off the DF during density fractionation. We assume that this small-size free OC is a small

410   fraction of the silt+clay OC as no small fragments of organic matter were visible and because the C:N ratios of the silt+clay

411   fraction are only slightly elevated compared to both the bulk and sand fraction (SI Table S1). For reference, the FLF has high

412   C:N reflecting the high OC content of this fraction (SI Table S1). Rather, the source of ^{14}C-enriched in the silt+clay relative

413   to the POC-free sand and bulk soil may be a result of higher surface area in the silt+clay for association of surface derived OC

414   with minerals.

415   Additionally, our TLE comparison on different size and density fractions highlights the important influence that method

416   selection has over experimental results. The mineral-associated TLE cycled more rapidly than the bulk soil no matter which

417   "mineral-associated" fraction (the silt+clay or the DF) was chosen. The $\Delta^{14}C$ values of TLE from the bulk, sand, and silt+clay

418   were indistinguishable from one another, possibly because the size fractionation scheme did not effectively separate distinct

419   lipid pools. However, the $\Delta^{14}C$ values of TLE from the DF were significantly more ^{14}C depleted than TLE from the silt+clay

420   size fraction (Fig. 6), suggesting there were older lipids in the DF relative to the silt+clay. However, more depleted ^{14}C values

421   found in the TLE from the DF compared to the silt+clay could have resulted from the DF being exposed to SPT and/or

422   ground after drying and before lipid extraction. It is possible that grinding the DF prior to lipid extraction increased the exposed

423   surface area and resulted in a larger fraction of old SOC or rock-derived OC being incorporated into the TLE than if the DF

had not been ground. Clearly, the approach used to fractionate soils influences experimental results and must be considered when trying to understand how the persistence of OC changes in different defined soil OC pools.

5 Conclusions and Continued soil radiocarbon compound class characterization

In this study, we characterized a soil carbon profile using compound-class ^{14}C analyses. We found that our extraction methods yielded fractions with ^{14}C signatures distinctly different from the bulk soil from which they were extracted. We found that in this grassland soil, the AA and the TLE fractions cycle more rapidly than the bulk soil throughout the soil profile. At each depth, the AI fraction is the oldest fraction and contains a combination of slowly cycling SOC and ancient petrogenic C. These results show that soil compound classes cycle differently than similar components in marine systems. Our results also show that mineral-associated SOC contains a mixture of carbon compounds with distinctly different ages and sources that drive turnover and persistence. Compound-specific ^{14}C approaches hold promise for improving our understanding of the chemical structure of soil organic carbon, as well as the connection between carbon degradation and preservation in soils. A molecule-resolved understanding of the relationship between compound classes and carbon persistence will also give insight into the fate and turnover time of specific organic biomarkers found in plant residues or the biomass of bacteria, fungi and microfauna. These techniques can also help to determine mechanisms promoting mineral stabilization of soil carbon, especially when combined with soil physical fractionation.

Results from this study highlight that radiocarbon measurements of specific organic compounds and compound classes in soil provide valuable insights into the persistence and decomposition rates of soil organic carbon. To improve our ability to model the future of soil carbon stocks and soil quality in the face of a changing global climate, we need further research that interrogates the composition, radiocarbon content, and cycling rates of soil organic carbon and mechanistically links these rates to physical and chemical drivers.

6 Acknowledgements

7 Supplemental Tables/Data Availability

A list of all radiocarbon data, stable carbon, and total OC values with a CAMS tracking number for each of the analyses

458   used in this publication.

459   **8 Author Contributions:** KJM, KMF, TABB, JP, and KEG conceptualized the study. KJM, KMF, TABB, JP secured funding

460   for the project. KEG designed the method and carried out the extractions with input from KJM, KMF, and TABB. CJL carried

461   out the density separations. MNR carried out the water extractions. JDK and MM ran the NMR experiments. KEG, KJM,

462   KMF interpreted the data. KEG prepared the paper with contributions of all co-authors.

463

464   **9 Competing interests.** The authors declare that they have no conflict of interest.

465

466

467   **References**

468

469   Agnelli, A., Trumbore, S. E., Corti, G., and Ugolini, F. C.: The dynamics of organic matter in rock fragments in soil
470   investigated by 14C dating and measurements of 13C, European Journal of Soil Science, 53, 147-159,
471   https://doi.org/10.1046/j.1365-2389.2002.00432.x, 2002.

472   Angst, G., Mueller, K. E., Nierop, K. G. J., and Simpson, M. J.: Plant- or microbial-derived? A review on the molecular
473   composition of stabilized soil organic matter, Soil Biology and Biochemistry, 156, 10.1016/j.soilbio.2021.108189, 2021.

474   Angst, G., John, S., Mueller, C. W., Kögel-Knabner, I., and Rethemeyer, J.: Tracing the sources and spatial distribution of
475   organic carbon in subsoils using a multi-biomarker approach, Scientific Reports, 6, 1-12, 2016.

476   Bahureksa, W., Tfaily, M. M., Boiteau, R. M., Young, R. B., Logan, M. N., McKenna, A. M., and Borch, T.: Soil Organic
477   Matter Characterization by Fourier Transform Ion Cyclotron Resonance Mass Spectrometry (FTICR MS): A Critical Review
478   of Sample Preparation, Analysis, and Data Interpretation, Environmental Science & Technology, 55, 9637-9656,
479   10.1021/acs.est.1c01135, 2021.

480   Baldock, J. A. and Preston, C. M.: Chemistry of Carbon Decomposition Processes in Forests as Revealed by Solid-State
481   Carbon-13 Nuclear Magnetic Resonance, in: Carbon Forms and Functions in Forest Soils, 89-117,
482   https://doi.org/10.2136/1995.carbonforms.c6, 1995.

483   Baldock, J. A., Oades, J. M., Nelson, P. N., Skene, T. M., Golchin, A., and Clarke, P.: Assessing the extent of decomposition
484   of natural organic materials using solid-state 13C NMR spectroscopy, Soil Research, 35, 1061-
485   1084, https://doi.org/10.1071/S97004, 1997.

486   Bartolome, J. W., James Barry, W., Griggs, T., and Hopkinson, P.: 367Valley Grassland, in: Terrestrial Vegetation of
487   California, edited by: Barbour, M., University of California Press, 0, 10.1525/california/9780520249554.003.0014, 2007.

488   Blattmann, T. M., Montluçon, D. B., Haghipour, N., Ishikawa, N. F., and Eglinton, T. I.: Liquid Chromatographic Isolation
489   of Individual Amino Acids Extracted From Sediments for Radiocarbon Analysis, Frontiers in Marine Science, 7,
490   10.3389/fmars.2020.00174, 2020.

491 Bour, A. L., Walker, B. D., Broek, T. A. B., and McCarthy, M. D.: Radiocarbon Analysis of Individual Amino Acids:
492 Carbon Blank Quantification for a Small-Sample High-Pressure Liquid Chromatography Purification Method, Analytical
493 Chemistry, 88, 3521-3528, 10.1021/acs.analchem.5b03619, 2016.

494 Broek, T. A. B., Ognibene, T. J., McFarlane, K. J., Moreland, K. C., Brown, T. A., and Bench, G.: Conversion of the
495 LLNL/CAMS 1 MV biomedical AMS system to a semi-automated natural abundance 14C spectrometer: system
496 optimization and performance evaluation, Nuclear Instruments and Methods in Physics Research Section B: Beam
497 Interactions with Materials and Atoms, 499, 124-132, 10.1016/j.nimb.2021.01.022, 2021.

498 Buettner, S. W., Kramer, M. G., Chadwick, O. A., and Thompson, A.: Mobilization of colloidal carbon during iron reduction
499 in basaltic soils, Geoderma, 221-222, 139-145, https://doi.org/10.1016/j.geoderma.2014.01.012, 2014.

500 Coppola, A. I., Wiedemeier, D. B., Galy, V., Haghipour, N., Hanke, U. M., Nascimento, G. S., Usman, M., Blattmann, T.
501 M., Reisser, M., Freymond, C. V., Zhao, M., Voss, B., Wacker, L., Schefuß, E., Peucker-Ehrenbrink, B., Abiven, S.,
502 Schmidt, M. W. I., and Eglinton, T. I.: Global-scale evidence for the refractory nature of riverine black carbon, Nature
503 Geoscience, 11, 584-588, 10.1038/s41561-018-0159-8, 2018.

504 De Troyer, I., Amery, F., Van Moorleghem, C., Smolders, E., and Merckx, R.: Tracing the source and fate of dissolved
505 organic matter in soil after incorporation of a 13C labelled residue: A batch incubation study, Soil Biology and
506 Biochemistry, 43, 513-519, https://doi.org/10.1016/j.soilbio.2010.11.016, 2011.

507 Douglas, P. M. J., Pagani, M., Eglinton, T. I., Brenner, M., Curtis, J. H., Breckenridge, A., and Johnston, K.: A long-term
508 decrease in the persistence of soil carbon caused by ancient Maya land use, Nature Geoscience, 11, 645-649,
509 10.1038/s41561-018-0192-7, 2018.

510 Dwivedi, D., Riley, W., Torn, M., Spycher, N., Maggi, F., and Tang, J.: Mineral properties, microbes, transport, and plant-
511 input profiles control vertical distribution and age of soil carbon stocks, Soil Biology and Biochemistry, 107, 244-259, 2017.

512 Eglinton, T. I., Galy, V. V., Hemingway, J. D., Feng, X., Bao, H., Blattmann, T. M., Dickens, A. F., Gies, H., Giosan, L.,
513 Haghipour, N., Hou, P., Lupker, M., McIntyre, C. P., Montlucon, D. B., Peucker-Ehrenbrink, B., Ponton, C., Schefuss, E.,
514 Schwab, M. S., Voss, B. M., Wacker, L., Wu, Y., and Zhao, M.: Climate control on terrestrial biospheric carbon turnover,
515 Proc Natl Acad Sci U S A, 118, 10.1073/pnas.2011585118, 2021.

516 Feng, X., Vonk, J. E., Griffin, C., Zimov, N., Montluçon, D. B., Wacker, L., and Eglinton, T. I.: 14C Variation of Dissolved
517 Lignin in Arctic River Systems, ACS Earth and Space Chemistry, 1, 334-344, 10.1021/acsearthspacechem.7b00055, 2017.

518 Feng, X., Benitez-Nelson, B. C., Montluçon, D. B., Prahl, F. G., McNichol, A. P., Xu, L., Repeta, D. J., and Eglinton, T. I.:
519 14C and 13C characteristics of higher plant biomarkers in Washington margin surface sediments, Geochimica et
520 Cosmochimica Acta, 105, 14-30, https://doi.org/10.1016/j.gca.2012.11.034, 2013.

521 Foley, M. M., Blazewicz, S. J., McFarlane, K. J., Greenlon, A., Hayer, M., Kimbrel, J. A., Koch, B. J., Monsaint-Queeney,
522 V., Morrison, K., Morrissey, E., Hungate, B. A., and Pett-Ridge, J.: Active populations and growth of soil microorganisms
523 are framed by mean annual precipitation in three California annual grasslands, Soil Biology and Biochemistry, 108886,
524 https://doi.org/10.1016/j.soilbio.2022.108886, 2022.

525 Galy, V., Peucker-Ehrenbrink, B., and Eglinton, T.: Global carbon export from the terrestrial biosphere controlled by
526 erosion, Nature, 521, 204-207, 10.1038/nature14400, 2015.

527 Galy, V., Beyssac, O., France-Lanord, C., and Eglinton, T.: Recycling of Graphite During Himalayan Erosion: A Geological
528 Stabilization of Carbon in the Crust, Science, 322, 943-945, doi:10.1126/science.1161408, 2008.

529 Gaudinski, J. B., Trumbore, S. E., Davidson, E. A., and Zheng, S.: Soil carbon cycling in a temperate forest: radiocarbon-
530 based estimates of residence times, sequestration rates and partitioning of fluxes, Biogeochemistry, 51, 33-69,
531 10.1023/A:1006301010014, 2000.

532 Gies, H., Hagedorn, F., Lupker, M., Montluçon, D., Haghipour, N., van der Voort, T. S., and Eglinton, T. I.: Millennial-age
533 glycerol dialkyl glycerol tetraethers (GDGTs) in forested mineral soils: 14C-based evidence for stabilization of microbial
534 necromass, Biogeosciences, 18, 189-205, 10.5194/bg-18-189-2021, 2021.

535 Gleixner, G.: Soil organic matter dynamics: a biological perspective derived from the use of compound-specific isotopes
536 studies, Ecological Research, 28, 683-695, 2013.

537 Grant, K. E., Hilton, R. G., and Galy, V. V.: Global patterns of radiocarbon depletion in subsoil linked to rock-derived
538 organic carbon, Geochemical Perspectives Letters, 25, 36-40, https://doi.org/10.7185/geochemlet.2312, 2023.

539 Grant, K. E., Galy, V. V., Haghipour, N., Eglinton, T. I., and Derry, L. A.: Persistence of old soil carbon under changing
540 climate: The role of mineral-organic matter interactions, Chemical Geology, 587, 10.1016/j.chemgeo.2021.120629, 2022.

541 Hagedorn, F., Saurer, M., and Blaser, P.: A 13C tracer study to identify the origin of dissolved organic carbon in forested
542 mineral soils, European Journal of Soil Science, 55, 91-100, https://doi.org/10.1046/j.1365-2389.2003.00578.x, 2004.

543 Hein, C. J., Usman, M., Eglinton, T. I., Haghipour, N., and Galy, V. V.: Millennial-scale hydroclimate control of tropical
544 soil carbon storage, Nature, 581, 63-66, 10.1038/s41586-020-2233-9, 2020.

545 Homyak, P. M., Blankinship, J. C., Slessarev, E. W., Schaeffer, S. M., Manzoni, S., and Schimel, J. P.: Effects of altered dry
546 season length and plant inputs on soluble soil carbon, Ecology, 99, 2348-2362, https://doi.org/10.1002/ecy.2473, 2018.

547 Hua, Q., Turnbull, J. C., Santos, G. M., Rakowski, A. Z., Ancapichún, S., De Pol-Holz, R., Hammer, S., Lehman, S. J.,
548 Levin, I., Miller, J. B., Palmer, J. G., and Turney, C. S. M.: ATMOSPHERIC RADIOCARBON FOR THE PERIOD 1950–
549 2019, Radiocarbon, 64, 723-745, 10.1017/RDC.2021.95, 2022.

550 Huang, Y., Bol, R., Harkness, D. D., Ineson, P., and Eglinton, G.: Post-glacial variations in distributions, 13C and 14C
551 contents of aliphatic hydrocarbons and bulk organic matter in three types of British acid upland soils, Organic Geochemistry,
552 24, 273-287, http://dx.doi.org/10.1016/0146-6380(96)00039-3, 1996.

553 Hwang, J. and Druffel, E. R. M.: Lipid-Like Material as the Source of the Uncharacterized Organic Carbon in the Ocean?,
554 Science, 299, 881-884, doi:10.1126/science.1078508, 2003.

555 Ishikawa, N. F., Itahashi, Y., Blattmann, T. M., Takano, Y., Ogawa, N. O., Yamane, M., Yokoyama, Y., Nagata, T., Yoneda,
556 M., Haghipour, N., Eglinton, T. I., and Ohkouchi, N.: Improved Method for Isolation and Purification of Underivatized
557 Amino Acids for Radiocarbon Analysis, Analytical Chemistry, 90, 12035-12041, 10.1021/acs.analchem.8b02693, 2018.

558 Jia, J., Liu, Z., Haghipour, N., Wacker, L., Zhang, H., Sierra, C. A., Ma, T., Wang, Y., Chen, L., Luo, A., Wang, Z., He, J.-
559 S., Zhao, M., Eglinton, T. I., and Feng, X.: Molecular 14C evidence for contrasting turnover and temperature sensitivity of
560 soil organic matter components, Ecology Letters, 26, 778-788, https://doi.org/10.1111/ele.14204, 2023.

561 Jobbágy, E. G. and Jackson, R. B.: THE VERTICAL DISTRIBUTION OF SOIL ORGANIC CARBON AND ITS
562 RELATION TO CLIMATE AND VEGETATION, Ecological Applications, 10, 423-436, https://doi.org/10.1890/1051-
563 0761(2000)010[0423:TVDOSO]2.0.CO;2, 2000.

564   Keiluweit, M., Bougoure, J. J., Nico, P. S., Pett-Ridge, J., Weber, P. K., and Kleber, M.: Mineral protection of soil carbon
565   counteracted by root exudates, Nature Climate Change, 5, 588-595, 2015.

566   Kleber, M., Sollins, P., and Sutton, R.: A conceptual model of organo-mineral interactions in soils: self-assembly of organic
567   molecular fragments into zonal structures on mineral surfaces, Biogeochemistry, 85, 9-24, 2007.

568   Kögel-Knabner, I.: The macromolecular organic composition of plant and microbial residues as inputs to soil organic matter,
569   Soil Biology and Biochemistry, 34, 139-162, https://doi.org/10.1016/S0038-0717(01)00158-4, 2002.

570   Kotanen, P. M.: Revegetation following Soil Disturbance and Invasion in a Californian Meadow: a 10-year History of
571   Recovery, Biological Invasions, 6, 245-254, 10.1023/B:BINV.0000022145.03215.4f, 2004.

572   Kuzyakov, Y., Bogomolova, I., and Glaser, B.: Biochar stability in soil: Decomposition during eight years and
573   transformation as assessed by compound-specific 14C analysis, Soil Biology and Biochemistry, 70, 229-236,
574   http://dx.doi.org/10.1016/j.soilbio.2013.12.021, 2014.

575   Lavallee, J. M., Soong, J. L., and Cotrufo, M. F.: Conceptualizing soil organic matter into particulate and mineral-associated
576   forms to address global change in the 21st century, Global Change Biology, 26, 261-273, https://doi.org/10.1111/gcb.14859,
577   2020.

578   Lechleitner, F. A., Baldini, J. U. L., Breitenbach, S. F. M., Fohlmeister, J., McIntyre, C., Goswami, B., Jamieson, R. A., van
579   der Voort, T. S., Prufer, K., Marwan, N., Culleton, B. J., Kennett, D. J., Asmerom, Y., Polyak, V., and Eglinton, T. I.:
580   Hydrological and climatological controls on radiocarbon concentrations in a tropical stalagmite, Geochimica et
581   Cosmochimica Acta, 194, 233-252, https://doi.org/10.1016/j.gca.2016.08.039, 2016.

582   Lehmann, J. and Kleber, M.: The contentious nature of soil organic matter, Nature, 528, 60-68, 10.1038/nature16069, 2015.

583   Lehmann, J., Hansel, C. M., Kaiser, C., Kleber, M., Maher, K., Manzoni, S., Nunan, N., Reichstein, M., Schimel, J. P., Torn,
584   M. S., Wieder, W. R., and Kögel-Knabner, I.: Persistence of soil organic carbon caused by functional complexity, Nature
585   Geoscience, 13, 529-534, 10.1038/s41561-020-0612-3, 2020.

586   Loh, A. N., Bauer, J. E., and Druffel, E. R. M.: Variable ageing and storage of dissolved organic components in the open
587   ocean, Nature, 430, 877-881, 10.1038/nature02780, 2004.

588   Lützow, M. v., Kögel-Knabner, I., Ekschmitt, K., Matzner, E., Guggenberger, G., Marschner, B., and Flessa, H.:
589   Stabilization of organic matter in temperate soils: mechanisms and their relevance under different soil conditions - a review,
590   European Journal of Soil Science, 57, 426-445, 10.1111/j.1365-2389.2006.00809.x, 2006.

591   Marin-Spiotta, E., Chadwick, O. A., Kramer, M., and Carbone, M. S.: Carbon delivery to deep mineral horizons in Hawaiian
592   rain forest soils, Journal of Geophysical Research: Biogeosciences, 116, 2011.

593   McFarlane, K. J., Torn, M. S., Hanson, P. J., Porras, R. C., Swanston, C. W., Callaham, M. A., and Guilderson, T. P.:
594   Comparison of soil organic matter dynamics at five temperate deciduous forests with physical fractionation and radiocarbon
595   measurements, Biogeochemistry, 112, 457-476, 10.1007/s10533-012-9740-1, 2013.

596   Mikutta, R., Mikutta, C., Kalbitz, K., Scheel, T., Kaiser, K., and Jahn, R.: Biodegradation of forest floor organic matter
597   bound to minerals via different binding mechanisms, Geochimica et Cosmochimica Acta, 71, 2569-2590, 2007.

598   Moe, L. A.: Amino acids in the rhizosphere: From plants to microbes, American Journal of Botany, 100, 1692-1705,
599   https://doi.org/10.3732/ajb.1300033, 2013.

Nuccio, E. E., Anderson-Furgeson, J., Estera, K. Y., Pett-Ridge, J., De Valpine, P., Brodie, E. L., and Firestone, M. K.: Climate and edaphic controllers influence rhizosphere community assembly for a wild annual grass, Ecology, 97, 1307-1318, 10.1890/15-0882.1, 2016.

Poeplau, C., Don, A., Six, J., Kaiser, M., Benbi, D., Chenu, C., Cotrufo, M. F., Derrien, D., Gioacchini, P., Grand, S., Gregorich, E., Griepentrog, M., Gunina, A., Haddix, M., Kuzyakov, Y., Kühnel, A., Macdonald, L. M., Soong, J., Trigalet, S., Vermeire, M.-L., Rovira, P., van Wesemael, B., Wiesmeier, M., Yeasmin, S., Yevdokimov, I., and Nieder, R.: Isolating organic carbon fractions with varying turnover rates in temperate agricultural soils – A comprehensive method comparison, Soil Biology and Biochemistry, 125, 10-26, https://doi.org/10.1016/j.soilbio.2018.06.025, 2018.

Pries, C. E. H., Ryals, R., Zhu, B., Min, K., Cooper, A., Goldsmith, S., Pett-Ridge, J., Torn, M., and Berhe, A. A.: The Deep Soil Organic Carbon Response to Global Change, Annual Review of Ecology, Evolution, and Systematics, 54, 375-401, 10.1146/annurev-ecolsys-102320-085332, 2023.

R Core Team: R: A language and environment for statistical computing., R Foundation for Statistical Computing [code], 2019.

Repasch, M., Scheingross, J. S., Hovius, N., Lupker, M., Wittmann, H., Haghipour, N., Gröcke, D. R., Orfeo, O., Eglinton, T. I., and Sachse, D.: Fluvial organic carbon cycling regulated by sediment transit time and mineral protection, Nature Geoscience, 14, 842-848, 10.1038/s41561-021-00845-7, 2021.

Rethemeyer, J., Kramer, C., Gleixner, G., Wiesenberg, G. L. B., Schwark, L., Andersen, N., Nadeau, M.-J., and Grootes, P. M.: Complexity of Soil Organic Matter: AMS 14C Analysis of Soil Lipid Fractions and Individual Compounds, Radiocarbon, 46, 465-473, 10.1017/S0033822200039771, 2004.

Rocci, K. S., Lavallee, J. M., Stewart, C. E., and Cotrufo, M. F.: Soil organic carbon response to global environmental change depends on its distribution between mineral-associated and particulate organic matter: A meta-analysis, Science of The Total Environment, 793, 148569, https://doi.org/10.1016/j.scitotenv.2021.148569, 2021.

Schmidt, M. W., Torn, M. S., Abiven, S., Dittmar, T., Guggenberger, G., Janssens, I. A., Kleber, M., Kögel-Knabner, I., Lehmann, J., and Manning, D. A.: Persistence of soil organic matter as an ecosystem property, Nature, 478, 49-56, 2011.

Shi, Z., Allison, S. D., He, Y., Levine, P. A., Hoyt, A. M., Beem-Miller, J., Zhu, Q., Wieder, W. R., Trumbore, S., and Randerson, J. T.: The age distribution of global soil carbon inferred from radiocarbon measurements, Nature Geoscience, 13, 555-559, 2020.

Sierra, C. A., Müller, M., and Trumbore, S. E.: Modeling radiocarbon dynamics in soils: SoilR version 1.1, Geoscientific Model Development, 7, 1919-1931, 10.5194/gmd-7-1919-2014, 2014.

Silveira, M. L., Comerford, N. B., Reddy, K. R., Cooper, W. T., and El-Rifai, H.: Characterization of soil organic carbon pools by acid hydrolysis, Geoderma, 144, 405-414, https://doi.org/10.1016/j.geoderma.2008.01.002, 2008.

Stoner, S., Trumbore, S. E., González-Pérez, J. A., Schrumpf, M., Sierra, C. A., Hoyt, A. M., Chadwick, O., and Doetterl, S.: Relating mineral–organic matter stabilization mechanisms to carbon quality and age distributions using ramped thermal analysis, Philosophical Transactions of the Royal Society A: Mathematical, Physical and Engineering Sciences, 381, 20230139, doi:10.1098/rsta.2023.0139, 2023.

Stuiver, M. and Polach, H. A.: Discussion Reporting of 14C Data, Radiocarbon, 19, 355-363, 10.1017/s0033822200003672, 1977.

637 Swain, D. L., Langenbrunner, B., Neelin, J. D., and Hall, A.: Increasing precipitation volatility in twenty-first-century
638 California, Nature Climate Change, 8, 427-433, 10.1038/s41558-018-0140-y, 2018.

639 Torn, M. S., Swanston, C. W., Castanha, C., and Trumbore, S. E.: Storage and Tunover of Organic Matter in Soil, in:
640 Biophysico-Chemical Processes Involving Natural Nonliving Organic Matter in Environmental Systems, edited by: Senesi,
641 N., Xing, B., and Huang, P. M., Wiley-IUPAC series in biopysico-chemical processes in environmental systems, John Wiley
642 & Sons, Inc., Hoboken, New Jersey, 219-272, 2009.

643 Trumbore, S.: Age of Soil Organic Matter and Soil Respiration: Radiocarbon Constraints on Belowground C Dynamics,
644 Ecological Applications - ECOL APPL, 10, 399-411, 10.2307/2641102, 2000.

645 Trumbore, S. E. and Harden, J. W.: Accumulation and turnover of carbon in organic and mineral soils of the BOREAS
646 northern study area, Journal of Geophysical Research: Atmospheres, 102, 28817-28830, 10.1029/97jd02231, 1997.

647 Trumbore, S. E. and Zheng, S.: Comparison of Fractionation Methods for Soil Organic Matter 14C Analysis, Radiocarbon,
648 38, 219-229, 10.1017/s0033822200017598, 1996.

649 Ukalska-Jaruga, A., Smreczak, B., and Klimkowicz-Pawlas, A.: Soil organic matter composition as a factor affecting the
650 accumulation of polycyclic aromatic hydrocarbons, Journal of Soils and Sediments, 19, 1890-1900, 10.1007/s11368-018-
651 2214-x, 2019.

652 van der Voort, T. S., Mannu, U., Hagedorn, F., McIntyre, C., Walthert, L., Schleppi, P., Haghipour, N., and Eglinton, T. I.:
653 Dynamics of deep soil carbon – insights from 14C time series across a climatic gradient, Biogeosciences, 16, 3233-3246,
654 10.5194/bg-16-3233-2019, 2019.

655 van der Voort, T. S., Zell, C. I., Hagedorn, F., Feng, X., McIntyre, C. P., Haghipour, N., Graf Pannatier, E., and Eglinton, T.
656 I.: Diverse Soil Carbon Dynamics Expressed at the Molecular Level, Geophysical Research Letters, 44, 11,840-811,850,
657 10.1002/2017gl076188, 2017.

658 Vogel, C., Mueller, C. W., Höschen, C., Buegger, F., Heister, K., Schulz, S., Schloter, M., and Kögel-Knabner, I.:
659 Submicron structures provide preferential spots for carbon and nitrogen sequestration in soils, Nature Communications, 5,
660 2014.

661 Vogel, J. S., Southon, J. R., Nelson, D. E., and Brown, T. A.: Performance of catalytically condensed carbon for use in
662 accelerator mass spectrometry, Nuclear Instruments and Methods in Physics Research Section B: Beam Interactions with
663 Materials and Atoms, 5, 289-293, https://doi.org/10.1016/0168-583X(84)90529-9, 1984.

664 von Lutzow, M., Kogel-Knabner, I., Ekschmitt, K., Flessa, H., Guggenberger, G., Matzner, E., and Marschner, B.: SOM
665 fractionation methods: Relevance to functional pools and to stabilization mechanisms, Soil Biology and Biochemistry, 39,
666 2183-2207, 2007.

667 Wang, X.-C. and Druffel, E. R. M.: Radiocarbon and stable carbon isotope compositions of organic compound classes in
668 sediments from the NE Pacific and Southern Oceans, Marine Chemistry, 73, 65-81, https://doi.org/10.1016/S0304-
669 4203(00)00090-6, 2001.

670 Wang, X.-C., Callahan, J., and Chen, R. F.: Variability in radiocarbon ages of biochemical compound classes of high
671 molecular weight dissolved organic matter in estuaries, Estuarine, Coastal and Shelf Science, 68, 188-194,
672 10.1016/j.ecss.2006.01.018, 2006.

673 Wang, X.-C., Druffel, E. R. M., Griffin, S., Lee, C., and Kashgarian, M.: Radiocarbon studies of organic compound classes
674 in plankton and sediment of the northeastern Pacific Ocean, Geochimica et Cosmochimica Acta, 62, 1365-1378,
675 https://doi.org/10.1016/S0016-7037(98)00074-X, 1998.

676

677